Available online at www.sciencedirect.com

ScienceDirect

Optics Communications 281 (2008) 2207–2212

OPTICS COMMUNICATIONS

www.elsevier.com/locate/optcom

Optical tweezers of programmable shape with transverse scattering forces

Alexander Jesacher *, Christian Maurer, Severin Fürhapter, Andreas Schwaighofer, Stefan Bernet, Monika Ritsch-Marte

Division for Biomedical Physics, Innsbruck Medical University, Müllerstraße 44, A-6020 Innsbruck, Austria

Received 13 November 2007; received in revised form 4 December 2007; accepted 4 December 2007

Abstract

We propose a non-holographic method to create line traps of arbitrary shape in the sample plane. Setting the phase gradient along theses lines gives control over the transverse forces acting on the confined particles. Phase structures, displayed on a spatial light modulator, are optically processed by a spiral phase filter and imaged onto the object plane of a microscope objective. The resulting bright line structures can be used to trap microparticles. Additionally, they exert transverse scattering forces, which can be exploited for inducing orbital motions or for creating "attracting" or "repelling" points, respectively. We give theoretical and experimental evidence that these scattering forces are proportional to the curvature of the line tweezers.

PACS: 42.30.Kq; 42.79.Kr; 42.79.Ci; 87.80.Cc

Keywords: Optical tweezers; Spatial filtering; Spatial light modulator; Spiral phase

1. Introduction

In the last decade, holographic or diffractive optical tweezers [1] have greatly enhanced the possibilities of manipulating microscopic particles with light. Diffractively created patterns of light can be used to trap and manipulate dielectric particles by intensity gradients. The generalized phase contrast (GPC) method has been introduced as an alternative to diffractive tweezers by Glückstad and co-workers [2]. Basically the method is based upon projecting a phase-contrast-filtered image of a computer-steered phase modulator display into the object plane of a microscope. Phase structures, displayed at the SLM panel, are directly transferred into intensity images by the phase-contrast filter. The technique offers high intensity efficiency and allows real-time steering, since moving of traps can be directly achieved by moving the corresponding trap structures on the light modulator panel. However, to date such a method cannot be used to shape the trapping beam into certain interesting mode structures, such as Laguerre–Gaussian beams, which in holographic setups can be used to transfer controlled transverse momentum to the trapped objects. A related method for micromanipulation, which was recently proposed by Guo et al. [3], makes use of a spiral phase filter [4], instead of a phase-contrast filter. The filter operation performed by the spiral phase filter represents a two-dimensional generalization of the Hilbert transform [5] and creates field amplitudes which are roughly proportional to the phase and amplitude gradients of the patterns displayed at the modulator panel [6]. Consequently, the edges of binary amplitude or phase structures appear strongly enhanced. However, probably the most interesting property of a light field created by spiral phase filtering is that it shows a specific phase profile that may give rise to transverse scattering forces on microparticles. Unlike forces caused by intensity gradients, scattering forces are generally not conservative, which allows, for

* Corresponding author.
E-mail address: Alexander.Jesacher@i-med.ac.at (A. Jesacher).

0030-4018/$ - see front matter © 2007 Elsevier B.V. All rights reserved.
doi:10.1016/j.optcom.2007.12.042

instance, the realization of orbital motion. An example for light fields creating such motion are Laguerre–Gaussian modes, which show a helical phase structure of the form $\exp[\mathrm{i}\theta]$, where θ is the azimuthal coordinate. The optical torque resulting from this helical phase acts as "optical spanner" [7,8] and can induce a directed flow of microparticles [9]. By modifying the helical phase profile of Laguerre–Gaussian modes, it is also possible to modify their circular shape [10].

In this paper we present the experimental realization and evaluation of *spiral phase* tweezers, as proposed by Guo et al. [3], which – without using holographic methods – combine advantages of the GPC method like the easy generation of arbitrary light structures and real-time steering with the possibility of transferring optical torque. We also demonstrate an interesting feature of this filter method, which has not been described in Ref. [3], namely that the transverse scattering forces are proportional to the curvature of the projected light patterns.

2. Properties of spiral phase filtered light fields

To understand the effects of the spiral phase filter, let us consider the point spread function (PSF) of the system. The PSF describes how a point source $\delta(\vec{r})$ is imaged by a given system. In "filter-less" imaging systems like telescopes, the PSF usually corresponds to the Airy function. Analogously, the point spread function of a spiral phase imaging system is represented by a diffraction limited optical vortex, which shows the same helical phase profile as the spiral filter. Its radial amplitude profile $f(r)$ can be described using Bessel and Struve functions [6,11].

When an extended object is imaged by a spiral phase imaging system, every single point of this object appears as a tiny optical vortex in the image plane (see Fig. 1). The interference of all vortices yields the complete spiral-filtered image. To achieve the resulting field at a certain point $\vec{P}$, one has to integrate the contributions of all vortices to the field at this point. For simplicity, let us assume that $\vec{P}$ coincides with the origin of our coordinate system, i.e., $\vec{P}=\vec{0}$. Then, the vortex located at an adjacent point $\vec{Q}=(r_Q,\phi_Q)$ contributes to the field in point $\vec{0}$ with $E_{\mathrm{in}}(r_Q,\phi_Q)f(r_Q)\exp[\mathrm{i}(\pi+\phi_Q)]$, where E_{in} is the original light field (see Fig. 1). Note that here the *geometric* angle ϕ_Q appears in the phase of the light field.

Thus one can express the total output field at point $\vec{0}$ as follows:

$$E_{\mathrm{out}}(\vec{0}) \propto \int_0^\infty \int_0^{2\pi} E_{\mathrm{in}}(r,\phi)f(r)\exp[\mathrm{i}\phi]r\,\mathrm{d}r\,\mathrm{d}\phi. \tag{1}$$

In practice, the extension of $f(r)$, i.e. the PSF, is usually much smaller than typical variations in E_{in}. In this case it is valid to expand the input light field in a Taylor series to first order:

$$\begin{aligned}E_{\mathrm{in}}(\vec{r}) &\approx E_{\mathrm{in}}(\vec{0}) + \vec{\nabla}E_{\mathrm{in}}(\vec{r})|_{\vec{0}}\cdot\vec{r}\\ &= E_{\mathrm{in}}(\vec{0}) + \left(\vec{g}_{\mathrm{A}}(\vec{0})\exp[\mathrm{i}\Psi_{\mathrm{in}}(\vec{0})] + i\vec{g}_{\mathrm{P}}(\vec{0})E_{\mathrm{in}}(\vec{0})\right)\cdot\vec{r},\end{aligned} \tag{2}$$

and to restrict the r-integration to a limited interval $[0,\rho]$, where ρ defines the approximate radius of the PSF. In the above equation, $\vec{g}_{\mathrm{A}}=\vec{\nabla}|E_{\mathrm{in}}|$ and $\vec{g}_{\mathrm{P}}=\vec{\nabla}\Psi_{\mathrm{in}}$ represent the amplitude and phase gradients of the complex field $E_{\mathrm{in}}=|E_{\mathrm{in}}|\exp[\mathrm{i}\Psi_{\mathrm{in}}]$. Inserting Eq. (2) into Eq. (1) yields

$$\begin{aligned}E_{\mathrm{out}}(\vec{0}) \propto{}& E_{\mathrm{in}}(\vec{0})\int_0^\rho\int_0^{2\pi}\exp[\mathrm{i}\phi]f(r)r\,\mathrm{d}r\,\mathrm{d}\phi\\ &+\exp[\mathrm{i}\Psi_{\mathrm{in}}(\vec{0})]\int_0^\rho\int_0^{2\pi}\vec{g}_{\mathrm{A}}(\vec{0})\cdot\vec{r}\exp[\mathrm{i}\phi]f(r)r\,\mathrm{d}r\,\mathrm{d}\phi\\ &+\mathrm{i}E_{\mathrm{in}}(\vec{0})\int_0^\rho\int_0^{2\pi}\vec{g}_{\mathrm{P}}(\vec{0})\cdot\vec{r}\exp[\mathrm{i}\phi]f(r)r\,\mathrm{d}r\,\mathrm{d}\phi.\end{aligned} \tag{3}$$

Because of the integration over $\exp[\mathrm{i}\phi]$, the first term is zero. Evaluating the other two terms results in:

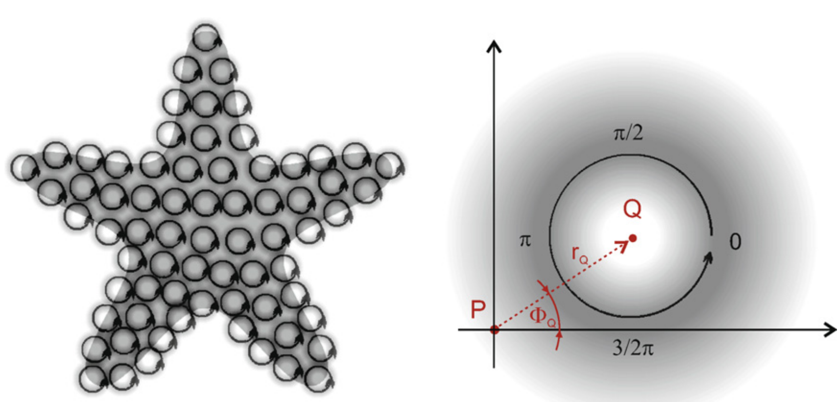

Fig. 1. Left: Every single point of the input light field (star) is imaged as diffraction limited optical vortex. Right: Sketch to visualize the contribution of an optical vortex located at $\vec{Q}$ to the field at point $\vec{P}$.

$$E_{\text{out}}(\vec{0}) \propto \exp[\mathrm{i}\Psi_{\text{in}}(\vec{0})]g_{\text{A}}(\vec{0})\Big\{\exp[\mathrm{i}\delta_{\text{A}}(\vec{0})]\int_0^{\rho}\int_0^{2\pi} f(r)r^2\,\mathrm{d}r\,\mathrm{d}\phi + \exp[-i\delta_{\text{A}}(\vec{0})]\int_0^{\rho}\int_0^{2\pi}\exp[\mathrm{i}2\phi]f(r)r^2\mathrm{d}r\,\mathrm{d}\phi\Big\} + \mathrm{i}E_{\text{in}}(\vec{0})g_{\text{P}}(\vec{0})\Big\{\exp[\mathrm{i}\delta_{\text{P}}(\vec{0})]\int_0^{\rho}\int_0^{2\pi} f(r)r^2\,\mathrm{d}r\,\mathrm{d}\phi + \exp[-\mathrm{i}\delta_{\text{P}}(\vec{0})]\int_0^{\rho}\int_0^{2\pi}\exp[\mathrm{i}2\phi]f(r)r^2\,\mathrm{d}r\,\mathrm{d}\phi\Big\}, \tag{4}$$

where δ_{A} and δ_{P} are the geometric polar angles of the amplitude and phase gradients. In the above equation, the integrals containing $\exp[\mathrm{i}2\phi]$ yield again zero, and the integral $\int_0^{\rho} f(r)r^2\,\mathrm{d}r$ yields a constant value. The filtered light field can finally be written as [6]

$$E_{\text{out}}(\vec{P}) \propto \exp[\mathrm{i}\Psi_{\text{in}}(\vec{P})]g_{\text{A}}(\vec{P})\exp[\mathrm{i}\delta_{\text{A}}(\vec{P})] + \mathrm{i}E_{\text{in}}(\vec{P})g_{\text{P}}(\vec{P})\exp[\mathrm{i}\delta_{\text{P}}(\vec{P})]. \tag{5}$$

This result is valid for an arbitrary point $\vec{P}$. It shows that the filtered light field is intense at amplitude and phase edges. In our experiments we restrict ourselves to phase structures, which do not absorb light and thus allow higher efficiency. Assuming E_{in} to be a pure phase function, Eq. 6 simplifies to

$$E_{\text{out}}(\vec{P}) \propto g_{\text{P}}(\vec{P})\exp[\mathrm{i}(\Psi_{\text{in}}(\vec{P}) + \delta_{\text{P}}(\vec{P}))]. \tag{6}$$

The filtered light field shows an interesting phase profile: its phase depends on δ_{P}, which is the geometric angle of the phase gradient. Consequently, straight edges will show a constant phase value, while a curve – where δ_{P} varies along its edge – will show a transverse phase gradient the amplitude of which is proportional to the curve bending. This property is also the basis of interferogram deconvolution in so-called "spiral interferometry" [12,13]. Using spiral-filtered light fields for micromanipulation, this means that curved parts within such structures exert transverse scattering force to microparticles, while straight lines do not.

3. Experimental setup

The probably simplest way of realizing spiral phase tweezers is to utilize a computer steered spatial light modulator (SLM) for displaying the phase structures and a separate static vortex filter element in a Fourier plane (see Fig. 2a), which for instance can be manufactured by photo-lithography [14]. Since such a filter element designed for a wavelength of 1064 nm (the wavelength of our trapping laser) was not available in our case, we decided to use one single SLM to display both, the structures to be filtered and the spiral phase filter. The two corresponding phase functions are placed side by side at the SLM panel. A sketch of the setup is shown in Fig. 2.

The structure pattern (pattern P_{S}) is fully illuminated by an expanded Ytterbium fiber laser at $\lambda = 1064$ nm. The diffracted light is subsequently focussed onto the spiral filter function (pattern P_{F}). Consequently, the Fourier Transform of P_{S} emerges at the filter function P_{F}. A sufficiently

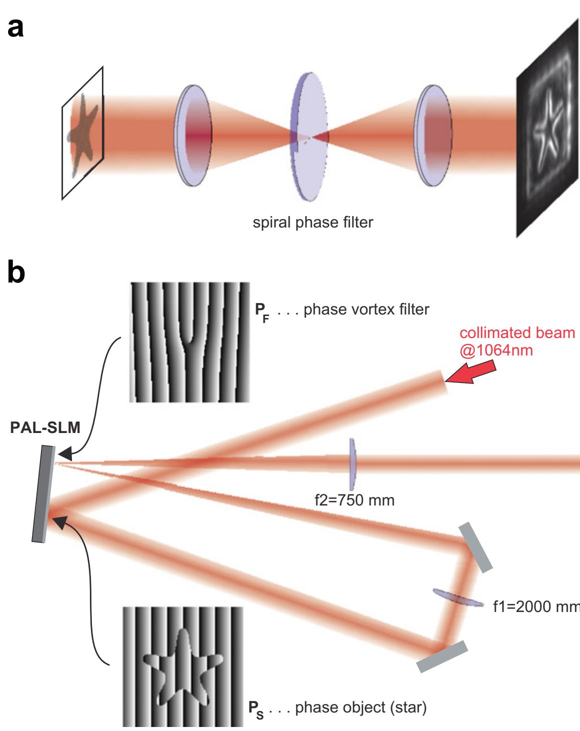

Fig. 2. (a) Principle of optical processing with a spiral phase filter. (b) Sketch of the experimental setup. One SLM displays both, the phase structure to be filtered and the spiral phase filter. The patterns are arranged side by side at the SLM panel. The gray values of the patterns represent phase values from 0 to 2π. Phase edges within P_{S} appear as bright lines in the spiral-filtered image under the microscope.

large focal length of the Fourier Transforming lens ($f_1 = 2000$ mm) prevents the display from being damaged by too high laser intensity and leads to a strongly downsized image of P_S in the microscope object plane. This is desired, if one wants to exploit the torque of the filtered light field. Finally the filtered light is coupled into a microscope objective by a 2-lens telescope.

The utilized SLM is a *HEO 1080* parallel aligned nematic device from *Holoeye Photonics AG* and shows a diffraction efficiency of approximately 40% at the wavelength of 1064 nm. The residual light is either absorbed (about 50%) or appears in other, undesired diffractive orders. To achieve a spatial separation of these orders from the desired light, we superpose both phase patterns by inclined phase planes (see Fig. 2). Regarding the limited phase modulation depth of the light modulator, the functions P_S and P_F are displayed modulo 2π radian:

$$P_S(x,y) = \mathrm{mod}2\pi[S(x,y) + k_S x], \tag{7}$$

$$P_F(x,y) = \mathrm{mod}2\pi[\arg(x + iy) + k_F x]. \tag{8}$$

There, $S(x,y)$ is the structure pattern – in our case a binary phase function. k_S and k_F are the gradients of the superposed inclined phase planes.

4. Experimental results

Fig. 3 shows various phase structures P_S, as they appear under the microscope, when the filter pattern P_F is a pure blazed grating without vortex. The dark lines dividing areas of different phase shift are explained by the low numerical aperture of our system (NA = 0.002): most of the light scattered from these lines is not caught by the subsequent optics, which lets them appear dark in the image. Adding a phase spiral to P_F results in strongly edge enhanced images (second row), as expected from Eq. (6). The squares surrounding the individual structures mark the boundaries of the pattern windows at the SLM panel.

Although the vortex filter is a pure phase filter and hence is supposed to preserve total power, it may practically not act intensity preserving in every case. Light, which is focussed into a small region around the singular filter center is strongly scattered [15] and may therefore be lost, if it is not captured by subsequent optics. Although this effect is of minor importance in specifically designed spiral phase imaging setups [4], it is strongly pronounced in the setup presented here, since the NA is very small. However, on

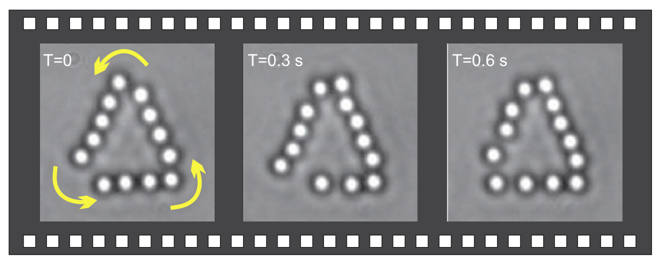

Fig. 4. Polystyrene beads (diameter = 750 nm), travelling in counterclockwise direction along the edges of a spiral-filtered phase triangle. The mean bead velocity is about 1.5 μm per second at total power of about 70 mW in the microscope object plane.

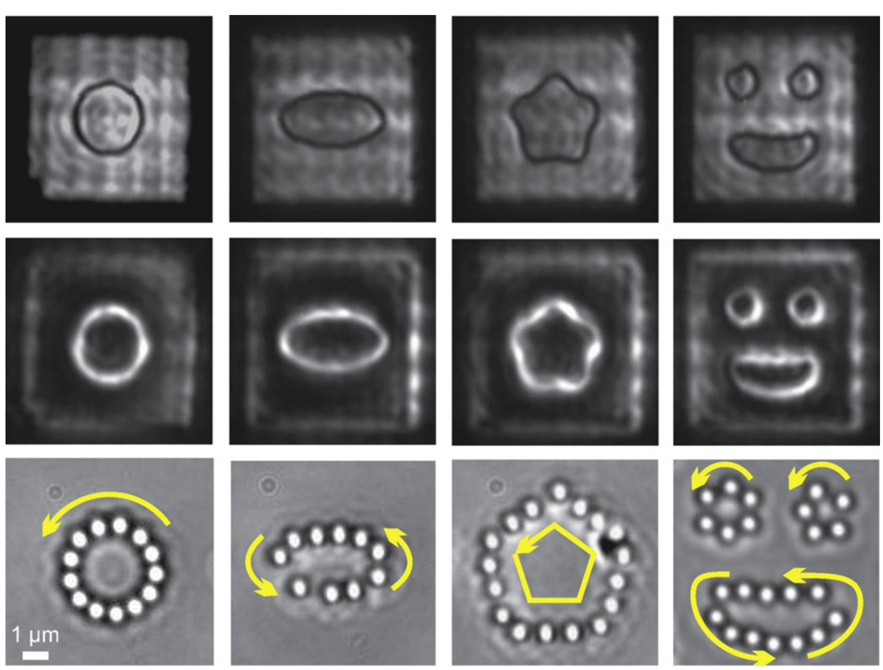

Fig. 3. Various binary phase structures, created by the SLM. The first row shows brightfield images of the structures as they appear under the microscope, if P_F is a pure grating without vortex. The images of the second row represent the spiral phase filtered patterns. As expected, the phase edges are strongly emphasized. As indicated by the images of the third row, they can act as optical traps for polystyrene microbeads (diameter 750 nm). The transverse scattering forces cause the particles to move along the bright lines. The total laser power in the microscope object plane was about 70 mW.

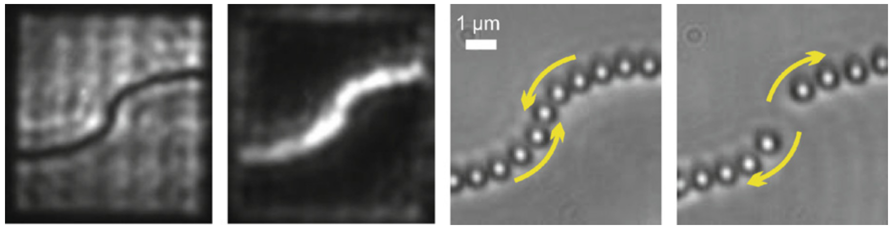

Fig. 5. Turning points represent points of attraction or repulsion, depending on the sign of the filter helicity. The total laser power in the object plane was about 90 mW.

the other hand this ensures a high degree of isotropy in the spiral-filtered images [6].

The images in the third row of the figure demonstrate the ability of the bright edges to act as optical traps. A water layer containing polystyrene microbeads (diameter 750 nm) was sandwiched between two glass coverslips, such that the layer thickness was about 20 µm. The beads were laterally trapped by the bright edges and simultaneously pressed onto the upper coverslip by scattering forces. The used objective is a *ZEISS Neofluar* with a magnification of 100 and a NA of 1.3.

The lateral phase gradients of the light fields at the structure edges cause the trapped beads to travel along the structure boundaries, as indicated by the arrows in Fig. 3. This effect is also demonstrated in Fig. 4 by means of movie snapshots. The observed motion only occurs when the structure is completely filled with microparticles, which is expected, since straight lines have a constant phase and do not exert transverse scattering forces. Thus, a single bead at any position on a straight line is not pushed by light forces into any direction. This has also been experimentally checked by creating straight line traps with the described method. On the other hand, if a closed line is "filled" with beads, the resulting closed chain always moves, since beads in a region without local tangential forces are pushed by neighbouring ones which are located at positions where a correspondingly higher momentum is transferred. Such a "closed chain" of beads also overcomes local stable trapping positions that can appear due to inhomogeneities of the light intensity distribution along a curve.

A further prediction of Eq. (6) is that the *sign* of the exerted optical torque depends on the *sign* of the line curvature. Hence, a turning point within a line trap should represent either a point of attraction or repulsion, depending on whether the vortex filter is of the form $\exp[i\phi]$ or $\exp[-i\phi]$. The experimental demonstration of this prediction is given in Fig. 5. The figure shows such a line trap, which was created by vortex filtering a specifically designed phase step (first and second image). As expected, a positive helicity caused a "compression" of the beads at the turning point, while a negative filter helicity led to a repulsion. Correspondingly, a soft object (like a red blood cell) trapped at such a point will experience a stretching or a compressing force, depending on the sign of the local curvature of its path.

5. Discussion

The presented experiments describe the, to our knowledge, first realization of optical tweezers shaped by a spiral phase filter, similarly as proposed by Guo et al. [3]. The setup makes use of one single phase modulator to create both, the trapping structures and the vortex filter. The setup shows some advantageous features of the GPC method [2], such as the straightforward non-holographic generation of light structures and real-time trap steering, with the additional feature of transverse momentum transfer. Our observations confirm that this transfer depends on the geometric curvature of the line trap. However, due to the structure of the vortex filter, the transverse phase gradient necessarily has – independent of the trapping structure – a mean value of $2\pi/L$, where L is the total length of the line trap. The transverse momentum transferred to polystyrene microparticles in water has, according to our observations, only a significant amplitude for relatively strong curvatures with radii in the range of 1 µm. Thus the presented method is probably only suitable for very specific tasks, but nevertheless represents a step towards the realization of arbitrarily shaped tweezers, where gradient and scattering forces can be adjusted independently.

Acknowledgements

This work was supported by the Austrian Science Foundation (FWF), Project Nos. P18051-N02 and P19582.

References

[1] J. Liesener, M. Reicherter, T. Haist, H.J. Tiziani, Opt. Commun. 185 (2000) 77.
[2] R.L. Eriksen, V.R. Daria, J. Glückstad, Opt. Express 10 (2002) 597.
[3] Cheng-Shan Guo, Yan Zhang, Yu-Jing Han, Jian-Ping Ding, Hui-Tian Wang, Opt. Commun. 259 (2006) 449.
[4] S. Fürhapter, A. Jesacher, S. Bernet, M. Ritsch-Marte, Opt. Express 13 (2005) 689.
[5] R.N. Bracewell, in: The Fourier Transform and its Applications, McGraw-Hill, New York, 1965.
[6] A. Jesacher, S. Fürhapter, S. Bernet, M. Ritsch-Marte, J. Opt. Soc. Am. A 23 (2006) 1400.
[7] N.B. Simpson, K. Dholakia, L. Allen, M.J. Padgett, Opt. Lett. 23 (1997) 52.
[8] A.T. O'Neil, I. MacVicar, L. Allen, M.J. Padgett, Phys. Rev. Lett. 88 (2002) 053601.

[9] K. Ladavac, D.G. Grier, Opt. Express 12 (2004) 1144.
[10] J.E. Curtis, D.G. Grier, Opt. Lett. 28 (2003) 872.
[11] S.N. Khonina, V.V. Kotlyar, M.V. Shinkaryev, V. Soifer, J. Mod. Opt. 39 (1992) 1147.
[12] S. Fürhapter, A. Jesacher, S. Bernet, M. Ritsch-Marte, Opt. Lett. 30 (2005) 1953.
[13] X.-C. Yuan, N. Zhang, S.H. Tao, J. Bu, J. Lin, Appl. Phys. Lett. 91 (2007) 171116.
[14] S.S.R. Oemrawsingh, J.A.W. van Houwelingen, E.R. Eliel, J.P. Woerdman, E.J.K. Verstegen, J.G. Kloosterboer, G.W. t Hooft, Appl. Opt. 43 (2004) 688.
[15] F.S. Roux, Opt. Commun. 223 (2003) 31.